(Received 10 June 2024, Accepted 4 August 2024, Scheduled 22 August 2024)

Nonlinear Testing-Based EMI Characterization of Wireless Communication Transmitter with Microwave Power Amplifier

Hongyu Du[1], Fayu Wan[1,*], Vladimir Mordachev[2], Eugene Sinkevich[2], Xiaohe Chen[3], Glauco Fontgalland[4], Dinh-Thuan Do[4], Samuel Ngoho[5], and Blaise Ravelo[1]

[1]*Nanjing University of Information Science & Technology (NUIST), Nanjing 210044, Jiangsu, China*
[2]*R&D Laboratory of EMC, BSUIR, Minsk, Belarus*
[3]*College of Information Science & Engineering, China University of Petroleum, Beijing, China*
[4]*School of Engineering, University of Mount Union, Alliance 44601, USA*
[4]*AFSCET, 151 Bd de l'Hôpital, Paris 75013, France*

ABSTRACT: An effective empirical method of EMI analysis for transceiver (Tx-Rx) system implemented with nonlinear (NL) microwave power amplifier (MPA) dedicated to wireless communication is developed. The nonlinearity is experimentally quantified by the MPA gain, P1dB, and third order intermodulation component via spectral response around 2.4 GHz 802.11b IEEE frequency band. The proof-of-concept represents the Tx-Rx system environment for wireless communication. The considered test signal emulates synchronization and physical broadcast different channels of downlink communication signals under QPSK modulation. The error vector magnitude (EVM) and signal-to-noise-ratio (SNR) due to the microwave Tx-Rx transmission undesirable EMI effect are assessed. Without MPA, the EVM and SNR of various channels fluctuate within a small range. Because of MPA nonlinearity, EMI becomes awfully significant due to the intermodulation generating SNR 20-dB decrease.

1. INTRODUCTION

Nowadays, the on wireless communication system evolves toward the spreading of 6G technologies [1]. However, electromagnetic compatibility (EMC) design researchers have to overcome significant open problems before the maturity of 6G wireless transceiver (TxRx) [1]. Remarkable EMC analyses of wireless systems were reported by the estimation of signal-to-noise ratio (SNR) [2, 3]. The effect of high-power electromagnetic interference (EMI) from switching amplifier operating with digital modulated signal was investigated [4]. Among the emphasized problems, appropriate solution must be developed against EMC and EMI challenges [5–7]. To deal with unintentional radio frequency interference (RFI) issues in wireless communication systems, some tentative approaches notably intended for the EMI reduction were proposed by exploring spread spectrum technique [8, 9] and pseudorandomized carrier frequency modulation [10]. A predictive approach of the impact of magnetic components was introduced for EMI suppression on the power amplifier (PA) baseband [11]. A millimeter-wave (mm-wave) gallium nitride (GaN) monolithic microwave integrated circuit (MMIC) Doherty power amplifier (DPA) based on an adaptive peak gate bias network with reconfigurable diodes is presented to improve linearity for EMI reduction [12].

It was found that the nonlinear (NL) effects of TxRx active components as power amplifiers constitute one of the main causes of RFI [13–15]. For example, the hardware impairments were caused by nonlinear power amplifiers [14]. An NL model of EMI-induced distortion phenomena was suggested with a circuit constituted by feedback CMOS operational amplifiers [15, 16]. Behind the EMI reduction approach, the mechanism can be understood more deeply with the consideration of nonlinear distortions, in particular, of modulated signals [17]. However, the EMI effect was performed notably with analysis, modelling, computation, and estimations of high-frequency harmonics distortion from transmitter (Tx) amplifier [18–22]. An innovative approach of intermodulation distortion estimation is developed with radio frequency (RF) component nonlinearities [23]. An analysis and design of third-order intermodulation (IM3) of a receiver (Rx) function is proposed [24].

In summary, most of the approaches to analyze the impact of nonlinearities on communication systems are achieved through modeling, simulation, and computation, which have limitations in real scenarios [25, 26], and therefore, more innovative characteristic approach for NL analysis is necessary for example by taking into account the interaction between component and system [27]. So far, the EMI-induced distortion remains a hot topic in the RF and communication engineering [28]. Therefore, the EMC design researchers are constantly looking for relevant prediction methods of EMI effects caused by amplifier nonlinearity [29]. An EMI virtual testing of electronic devices was developed according to the EMC requirements [30]. Despite the accomplished experimental techniques [31], further improvement of EMC pre-compliance testing's notably to the 5G and 6G TxRx components is ongoing.

In existing approaches, many research evaluations focus on bit error rate (BER) to analyze the impact of nonlinearities on

* Corresponding author: Fayu Wan (fayu.wan@nuist.edu.cn).

communication systems; however, BER is only a measure of the number of bit errors that actually occur during transmission and does not directly reflect the modulation quality of the signal or the overall distortion of the signal. In high-quality systems, BER is so low that more data needs to be transmitted to capture enough errors for statistical analysis. This makes BER testing more expensive in terms of time and resources.

EVM and SNR provide multi-dimensional performance information: EVM measurements provide a comprehensive picture of the quality of the modulated signal, including amplitude and phase errors, while SNR measures the strength of the signal relative to the level of noise, providing information on signal clarity. Combined, these two provide a more comprehensive assessment of the signal's transmission quality. EVM and SNR provide instant feedback, which is useful for debugging and optimizing the system.

In the present research work, an EMI characterization test of microwave power amplifier (MPA) nonlinearity including P1dB and IM3 assessment with Quadrature Phase Shift Keying (QPSK) communication signal is developed. The IM3 is characterized from double frequency test system [32, 33]. The developed technique includes innovative SNR assessment by means of error vector magnitude (EVM) and constellation diagram from 802.11b IEEE standard communication signal.

The paper is organized in four main sections as follows:

- Section 2 describes the MPA device under test (DUT) and the NL test plan.
- Section 3 introduces the empirical polynomial model of the MPA gain.
- Section 4 develops the IM3 measurement technique. The experimental results around the 2.4 GHz carrier frequency are discussed.
- Section 5 analyzes the EMI effect on wireless communication system operating with QPSK modulation signal by taking into account the MPA nonlinear effects.
- Section 6 is the final conclusion.

2. DESCRIPTION OF MPA DUT AND MEASUREMENT PLAN

The present section introduces the DUT and the measurement plan considered for the present NL and EMI characterization of wireless communication signals.

2.1. Experimental Test Objective Description

The main device under test (DUT) for this experiment is AV3860C MPA, as shown in Figure 1. The AV3860C microwave power amplifier is a broadband high-power microwave amplifier known for its convenience in portability, ease of operation, and wide frequency bandwidth. Its notable features include high amplification and large output power within the frequency range of 0.8 GHz to 20 GHz.

The aim of this experiment is to adjust the output signal of the signal generator to change the radio frequency input of the power amplifier. Simultaneously, record the RF output signal power to the EMI Rx. This data is then used to plot the input-output curve of the power amplifier. Subsequently, the gain and P1dB compression point of the power amplifier are calculated.

FIGURE 1. AV3860C MPA.

2.2. Signal Generator and EMI Rx

The equipment used in this measurement includes an RF signal generator, a microwave power amplifier, an attenuator, an EMI Rx, and several coaxial cables with adapters. The signal generator used in the measurement is Agilent N9310A, capable of generating signals from 9 kHz to 3 GHz. It supports both analog modulation and IQ modulation. The N9310A RF signal generator is depicted in Figure 2(a). The EMI Rx used in this experiment is the Agilent N9038A, as shown in Figure 2(b).

This Rx is capable of displaying signal spectra from 20 Hz to 26.5 GHz. It features fast FFT scanning, enabling efficient time-domain scans and ensuring short overall scanning times. In this measurement, a 20 dB attenuator with SMA connectors illustrated by Figure 2(c) is utilized. This attenuator can withstand a power up to 20 W, providing a 20 dB attenuation.

The three items of the performed measurement using the described apparatuses are described in the following subsections.

2.3. Section One: MPA Input and Output Performance Measurement

The different apparatuses are specified as follows:

(1) This measurement uses an AV3860C microwave power amplifier, with the saturated output power of over 29 dBm (input signal frequency 0.8 GHz $\sim$ 20 GHz).

(2) Input level is limited to 10 dBm.

(3) Measurement setup includes: signal generator, microwave power amplifier, EMI Rx, coaxial attenuator, coaxial transmission line, etc.

(4) Measurement of losses in attenuator and coaxial line connections: Connect the signal generator, attenuator, and EMI Rx in sequence. Power on the devices. Start the signal generator and EMI Rx. Set the input signal to 0 dBm, frequency to $f_0 = 2.4$ GHz, and adjust appropriate Res. BW (resolution bandwidth) and span (observation band-

FIGURE 2. (a) N9310A RF signal generator and (b) Agilent N9038A EMI Rx.

width). Record the absolute value of the Rx signal spectrum peak as the loss of the coaxial line and attenuator.

(5) Measure the linearity of the microwave power amplifier: Turn off the output of signal generator and reconnect the instruments in sequence using the coaxial line: signal generator — RF power amplifier — coaxial attenuator — EMI Rx. Then, adjust the signal generator output power from -30 dBm to 10 dBm and simultaneously record the output signal power of the source and the input signal power of the Rx. Finally, the sum of the attenuator and coaxial line losses in the Rx's input signal represents the output signal power of the power amplifier. Because the coaxial line connecting the signal generator and power amplifier is relatively short and has small losses, the output signal of the signal source can be considered as the input signal of the power amplifier, neglecting the losses of the coaxial line. By plotting the input-output curve of the power amplifier, its linearity can be observed, and the gain and P1dB compression point of the power amplifier can be calculated.

(6) Fitting the power amplifier memory polynomial model using least squares method: the expression for the traditional memory polynomial model can be written as follows:

$$z(n) = \sum_{i=0}^{m} \sum_{j=0}^{q} a_{ij} x(n-j)|x(n-j)|^i \qquad (1)$$

where $x(n)$ represents the input signal of the power amplifier, $z(n)$ the output signal of the power amplifier, m the polynomial order, and q the memory depth of the polynomial. By substituting the input-output data obtained from the above measurement into the memory polynomial model, calculate the least squares solution of this system of equations to obtain the polynomial coefficients a_{ij} $(0 \leq i \leq m,\ 0 \leq j \leq q)$.

(7) Organize the data and draw conclusions.

2.4. Section 2: MPA IM3 Measurement

The main constituting blocks for this test are:

(1) Preparation of measurement conditions: Prepare two signal generators, a power divider, microwave power amplifier, EMI Rx, coaxial attenuator, coaxial transmission line, etc.

(2) Measurement of attenuator and coaxial line losses: Connect the two signal generators through the combiner to the attenuator and the Rx. Power on the signal generators and EMI Rx. Set the signal frequency f_1 of one signal generator to f_0 and f_2 of the other signal generator to 2.401 GHz. Both signal generators output signals ranging from -30 dBm to 20 dBm. Adjust appropriate Res BW and Span. Record the power levels of the Rx signal spectrum at frequencies f_1 and f_2. The absolute difference between these power levels and the output signal of the signal sources represents the losses in the attenuator and coaxial line. Average the losses from multiple measurements.

(3) Measurement of IM3 components of the MPA: Turn off the signal outputs of the two generators. Connect the two signal generators through the combiner to the power amplifier, attenuator, and Rx. Power on the amplifier, signal generators, and EMI Rx. Set the signal source frequency as in Measurement (2). Start from -30 dBm and gradually increase the signal source power until IM3 components appear in the Rx (intermodulation frequencies are $2f_1 - f_2$ and $2f_2 - f_1$). Then, increase the signal source power in 1 dBm steps until an appropriate power level within the input power limit of the power amplifier. Simultaneously record the power levels of the IM3 components in the Rx's signal spectrum. The sum of these intermodulation components and the losses measured in Measurement (2) represents the power levels of the power amplifier's IM3 components. Plotting the input-output curve of the fundamental signals from Measurement (1), and the IM3 components from Measurement (2) allows the calculation of the power amplifier's IM3 point.

(4) Shutdown and data analysis: Power off and disconnect all instruments. Organize the data and draw conclusions based on the IP3 calculation and analysis of the power amplifier's behaviour under different input conditions.

2.5. Section 3: Measurement of the Impact of MPA NL Characteristics on Wireless Communication System Performance

The main preparations for this test are:

(1) Preparations of measurement conditions: Prepare instruments including a computer with Windows 10, Agilent N5172B EXG vector signal generator, AV3860C microwave power amplifier, KEYSIGHT MXA signal analyzer N9020B, etc.

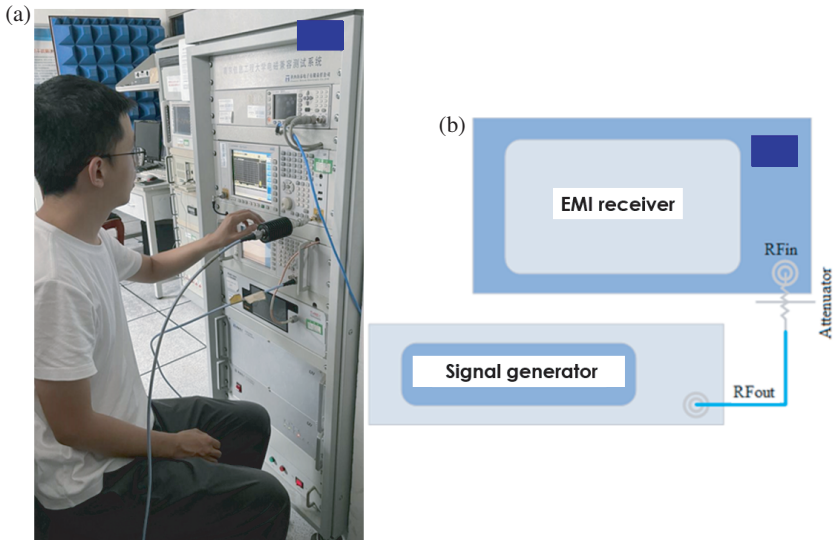

FIGURE 3. (a) The tester measures the attenuation at the amplifier output. (b) Diagram of MPA RF output attenuation measurement.

(2) Direct connection wireless communication quality measurement of signal generator and signal analyser: Connect the signal generator and analyzer directly through a coaxial cable. Use the computer to load signal source configuration files into the signal generator. Set the input signal as FDD downlink signal with f_0. The initial input signal power of the signal analyser is -30 dBm. Start the KEYSIGHT signal analyser's VSA software. Set observation frequency, bandwidth, and signal type. Set modulation type as QPSK. Signal generator output power range is the same as in Measurement (1) (starting from -30 dBm). Refresh VSA, observe changes in metrics such as EVM, constellation diagram, spectrum, etc. Save measurement data.

(3) Communication quality measurement through amplifier and signal analyser: Turn off the signal generator output. Insert the power amplifier (with an attenuator if necessary) between the signal generator and analyser. Repeat the measurement steps from Measurement (2). Compare the measurement results with the data from the previous two measurements to explore the impact of power amplifier nonlinear characteristics on wireless communication quality.

(4) Shutdown and data analysis: Power off and disconnect all instruments. Organize the data and draw conclusions based on the comparison of communication quality metrics under different measurement conditions.

3. EMPIRICAL MODELLING OF MPA NONLINEARITY GAIN

The NL measurement results of the MPA are examined in the present section.

3.1. MPA RF Input-Output Measurement Setup

The attenuation in the coaxial cable connecting the power amplifier output to the EMI Rx cannot be neglected, especially considering its length. Figure 3(a) shows the measurement personnel conducting attenuation measurements on the coaxial cable at the power amplifier output. Figure 3(b) shows block diagram of the attenuation measurement at the RF output of the MPA.

The signal generator and Rx are connected through a long coaxial cable with an attenuator. The signal generator's output signal is set to f_0, 0 dBm. Press the RF on/off button on the signal generator to output the signal. Set the Rx's spectrum center frequency to 2.4 GHz, Res BW to 30 kHz, VBW to 200 kHz, and observation bandwidth to 6.033 MHz. Press the Peak Search button to record the peak value of the Rx's spectrum at f_0. The difference between this peak value and the signal power from the signal source represents the attenuation from the power amplifier's RF output to the Rx. After measurement, the amplitude of the Rx's spectrum is -33.2 dBm. Therefore, the combined attenuation from the long coaxial cable and the attenuator is 33.2 dB (at f_0).

After completing the attenuation measurement, press the RF on/off button on the signal generator to turn off the signal output. Reconnect the cables according to the configuration shown in Figure 4(a). Draw the RF input-output measurement diagram of the power amplifier using Visio, as shown in Figure 4(b). Due to the relatively short length of the coaxial cable from the signal generator to the RF input of the amplifier, the losses in this short coaxial cable are not considered in this measurement. The output signal from the signal generator is considered as the RF input signal for the power amplifier. The attenuation from the power amplifier's RF output to the Rx is 33.2 dB. The signal generator output is adjusted from -30 dBm with intervals of 5 dBm up to -5 dBm. Then, it is adjusted from -4 dBm with 1 dBm intervals up to 10 dBm (narrowing the measurement intervals near the 1 dB compression point). The peak power of the Rx spectrum corresponding to the signal generator's output is recorded. The RF output signal power of the power amplifier is the measured peak power plus the attenuation from the long coaxial cable and the attenuator.

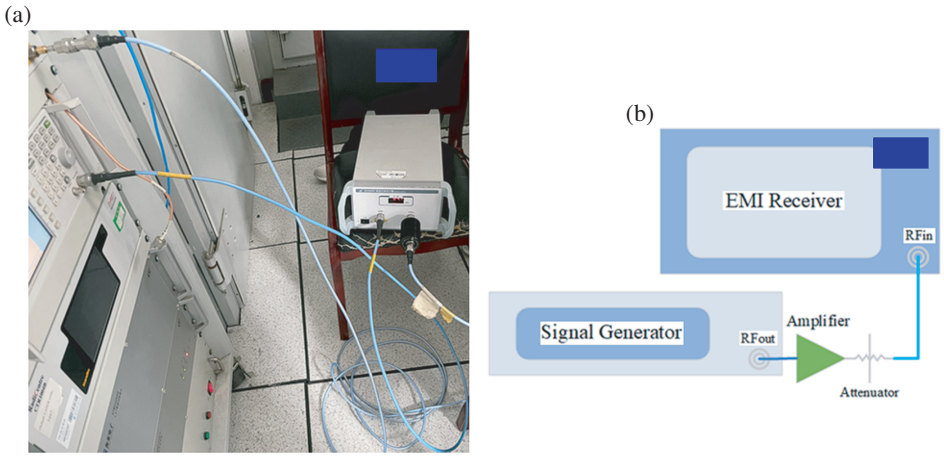

FIGURE 4. RF input-output measurement (a) photograph and (b) illustrative diagram with MPA (light blue represents coaxial cable).

TABLE 1. MPA Input & Output Data @ f_0.

P_{in} (dBm)	P_{out} (dBm)	P_{out_ideal} (dBm)	$P_{out\_ideal} - P_{out}$ (dBm)	Gain (dB)
−30	4.3	4.3	0	34.3
−25	9.3	9.3	0	34.3
−20	14.3	14.3	0	34.3
−15	19.3	19.3	0	34.3
−10	24.3	24.3	0	34.3
−5	29.2	29.3	0.1	34.2
−4	30.3	30.3	0	34.3
−3	31.3	31.3	0	34.3
−2	32.3	32.3	0	34.3
−1	32.9	33.3	0.4	33.9
0	33.8	34.3	0.5	33.8
1	34.32	35.3	0.98	33.32
2	35.05	36.3	1.25	33.05
3	35.65	37.3	1.65	32.65
4	36.13	38.3	2.17	32.13
5	36.49	39.3	2.81	31.49
6	36.77	40.3	3.53	30.77
7	36.98	41.3	4.32	29.98
8	37.21	42.3	5.09	29.21
9	37.41	43.3	5.89	28.41
10	37.53	44.3	6.77	27.53

3.2. Discussion on MPA RF Input-Output Results

The input and output data of the power amplifier are shown in Table 1. Based on the input and output data of the power amplifier, the ideal output signal corresponding to an increase in the input signal, as well as the compression point and gain of the power amplifier, can be calculated. Plotting the power amplifier's input and output curves and gain from the data in the table above, as shown in Figure 5, the gain of the power amplifier remains relatively constant at 34.3 dB between input signals of −30 dBm and −2 dBm. The output signal rises steadily in this range, showing a linear amplification effect. However, when the input signal exceeds −2 dBm, the power amplifier exhibits nonlinear characteristics.

The gain starts to decline, and the P1dB compression point is approximately at an input signal of 1 dBm (with a compression value of 0.98 dB). The increase in output signal power becomes less steep. For input signals greater than 5 dBm, the gain decreases nearly linearly. Within the power amplifier's tolerance range, the maximum output power is 37.53 dBm.

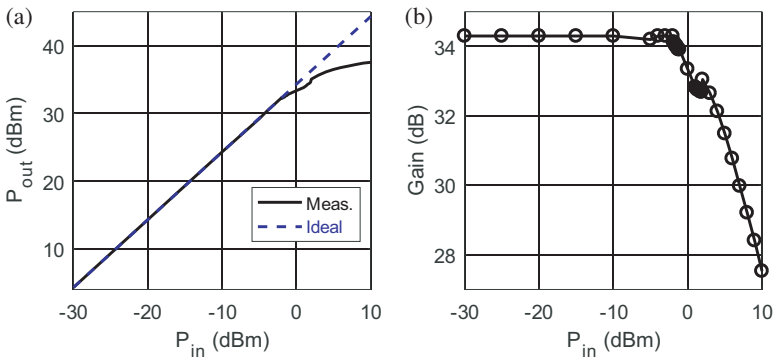

FIGURE 5. MPA output power and Gain vs input power.

TABLE 2. Specifications of SG and PWS shown by Fig. 7.

Description	Reference	Name	Value
SG_2	Agilent E8257D PSG ASG	BW	250 kHz–40 GHz
		Output power	17 dBm @ 40 GHz
		Modulation	AM-FM-phase-pulse modulation
PWC	Mini-Circuits ZFRSC-123+	Max. frequency	12 GHz
		Pmax	28.7 dBm

3.3. NL Empirical Polynomial Model

The traditional memory polynomial is a type of polynomial that incorporates memory effects and is used to represent the dynamic nonlinearity of RF power amplifiers. Its mathematical expression is given by Equation (1). Substituting the input-output data obtained from Table 1 into the memory polynomial model, we can obtain a system of equations with unknowns a_{ij} $(0 \leq i \leq m,\ 0 \leq j \leq q)$:

$$[X] \times [a] = [z] \tag{2}$$

X is a matrix formed by input signals, a a column vector composed of a_{ij}, and z a column vector formed by output signals. From Equation (2), we obtain the system of normal equations:

$$[X]^T \times [X] \times [A] = [X^T] \times [z] \tag{3}$$

Calculating the least squares solution of this system of equations will yield the polynomial coefficients unknowns a_{ij} $(0 \leq i \leq m,\ 0 \leq j \leq q)$. According to Ohm's law, the signal amplitude is equal to the square root of the signal power multiplied by the resistance. The characteristic impedance is 50 Ω, so according to Table 1, when the polynomial order is 5, and the memory depth is 6, with converting dBm to voltage (in V) the coefficients of the memory polynomial are computed using MATLAB. Figure 6 shows the comparison between the power amplifier input-output curve obtained through polynomial fitting with the aforementioned coefficients and the measured power amplifier input-output data.

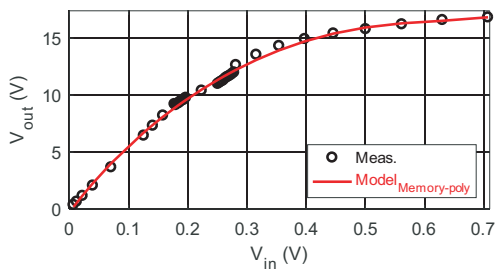

FIGURE 6. The fitted power amplifier input-output data and the measured power amplifier input-output data.

4. MPA NL EXPERIMENTATION METHODOLOGY

The present section describes the experimental setup and also the analysis of the NL characterization results of the proof-of-concept (POC) device represented by the considered MPA.

4.1. IM3 Experimental Setup Description

To assess the MPA IM3 components, two Signal Generators (SGs), SG_1 and SG_2, operating two different close enough frequencies $f_1 = f_0$ and $f_2 = 2.401$ GHz (by assuming $f_1 \ll 2f_2$ and $f_2 \ll 2f_1$) were considered. In difference to the previous case, the experimental setup was changed by using a power combiner (PWC) as illustrated by Figure 7. The PWC and the additional analog SG SG_2 specifications are addressed by Table 2.

By turning off the two SG outputs, the IM3 components measurement was performed by connecting the SGs, PWC, attenuator, and EMI Rx. The input signal power was set from $P_{in,\min}$ and gradually increased until IM3 components were identified at frequencies:

$$\begin{cases} f_a = 2f_1 - f_2 \\ f_b = 2f_2 - f_1 \end{cases} \tag{4}$$

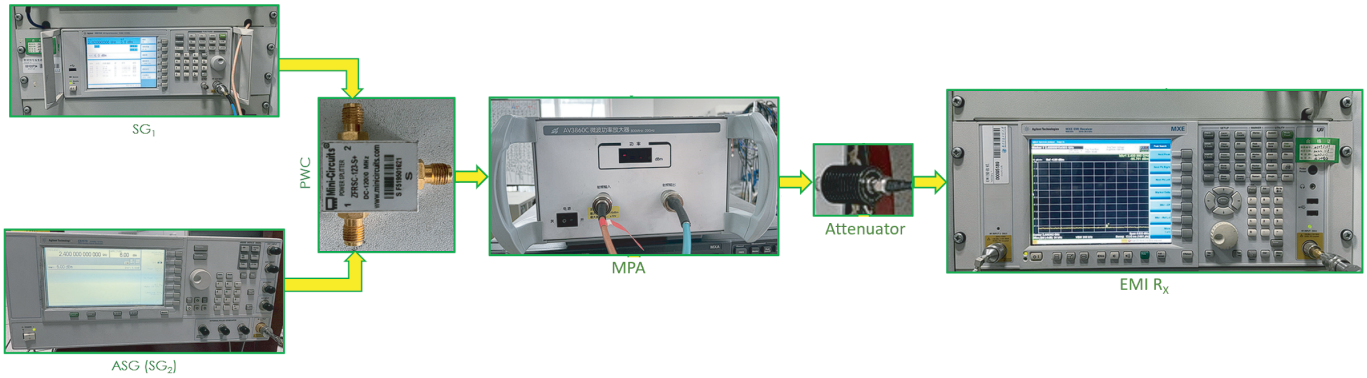

FIGURE 7. Illustrative diagram of IM3 Tx-Rx attenuation measurement setup.

The input signal source amplitude was increased by 1 dBm steps until an appropriate power level within the MPA input power limit was achieved. Thus, the power levels of the IM3 components were simultaneously recorded in the Rx signal spectrum. The sum of these components and attenuation losses represents the MPA IM3 components power levels.

Then, the input-output curve of the fundamental signals was plotted from measurement highlighted by Figure 7. Test results can be used to calculate MPA IIP3 and OIP3. Then, the shut-down and data analysis were proceeded by powering off and disconnect all instruments. The input signal level for both SGs, SG_1 and SG_2, were measured and varied between -30 dBm and 20 dBm.

4.2. Discussion on Experimented IM3 Results

Set the EMI Rx spectrum center frequency to f_0, the resolution bandwidth to 30 kHz, the view bandwidth to 200 kHz, and the observation bandwidth to 6.033 MHz to record the results. The output signal peak values at f_1 and f_2 are recorded in the EMI Rx spectrum. The difference between these peak values and the corresponding SG signal power indicates the attenuation measured by IM3 components. Since the attenuation from the MPA output to the Rx EMI is 33.2 dB, the attenuation of the SG to the input is 7.71 dB for signal f_1 and 8.04 dB for signal f_2. The test was performed by adjusting the SG output from -30 dBm in 5 dBm intervals until the IM3 components was observed on the EMI Rx and the SG output was gradually increased by 1 dBm. Peak powers at $f_a = 2.399$ GHz, f_1, f_2, and $f_b = 2.402$ GHz are obtained, and the peak power values are added to the output power to represent 33.2 dB. Since the spectrum of f_a is close to the spectrum of f_1, the f_b input can be considered as f_1 minus 7.71 dB of attenuation. Similarly, the f_b input can be considered as f_2 minus 8.04 dB of attenuation. A comparison of the MPA's IM3 components measured data (plotted in solid lines) with the computed data (plotted in dashed lines) can be obtained from Figure 8.

The results were computed by using the least squares method (LSM) to fit the linear amplification region of the IM3 components. By utilizing MATLAB, we can find the intersection points of the two IM3 components with the ideal amplification

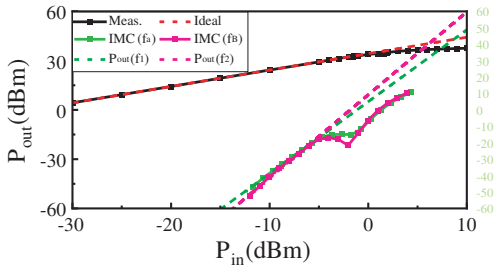

FIGURE 8. Comparison of measured and calculated IM3 components.

curve of the amplifier which represents the IM3 indicated by Table 3.

Since the slope of the ideal curve for the IM3 component f_a is closer to the theoretical slope of 3, this study considers IIP3 and OIP3 to be (8.69 dBm, 42.99 dBm).

TABLE 3. Measured IM3 components at f_a and f_b.

Frequency	Input (dBm)	Output (dBm)
f_a	8.69	42.99
f_b	5.79	40.09

5. EMI ANALYSIS WITH WIRELESS COMMUNICATION QPSK MODULATION SIGNAL

In the present section, the MPA NL effect on the quality of 802.11b IEEE communication is investigated. The Tx-Rx EVM and SNR influenced by the MPA NLT are assessed by multi-channel downlink communication with Quadrature Phase Shift Keying (QPSK) modulation.

5.1. Description of the EMI Assessment Experimental Setup with QPSK Modulation Communication

Figure 9 explains the experimental setup to perform the EMI analysis. As illustrated in this diagram, in this study case, a vector SG (VSG) and a vector signal analyzer (VSA) were used as Tx and Rx terminals. The EMI analysis methodology depends on the consideration QPSK signal new radio frequency-

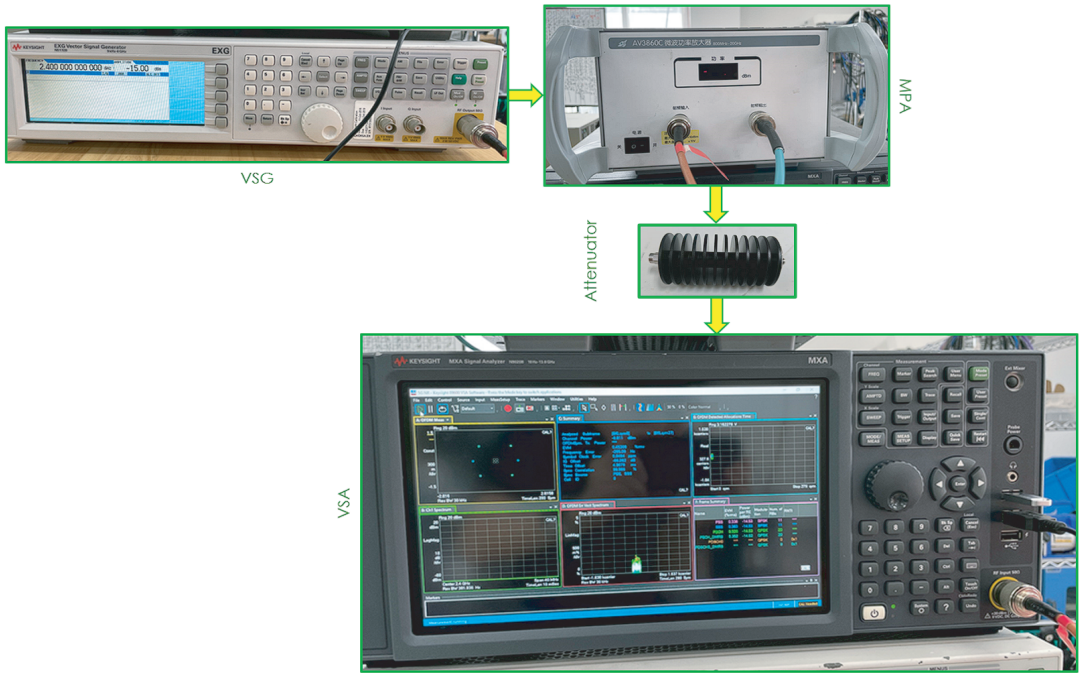

FIGURE 9. Measurement equipment setup.

division duplexing (FDD) standard specifications modulated at f_0 which is assumed to represent a wireless communication study case.

The observed data were interpreted with signal analyzer (SA). The measurement methodology can be summarized by the following steps:

- Step 1: Load the FDD signal source configuration file into Signal Studio software.
- Step 2: Configure the modulation scheme as QPSK in Signal Studio and set the initial signal power to -30 dBm.
- Step 3: Control the SG output using Signal Studio software and do not connect the MPA and attenuator.
- Step 4: Input the signal into the VSA.
- Step 5: Configure the SA parameters such as signal type, resolution BW, span width, and reference level.
- Step 6: Observe changes in the SA constellation diagram and spectrum.
- Step 7: Capture and save the data from the SA by checking the VSA software interface for measurement data shown by Figure 9.

5.2. Discussion on the MPA NLT Influence on the Constellation Diagram

The present empirical study is based on the wireless communication signal operating at f_0 with QPSK modulation. Based on the measured constellation diagram displayed in Figure 10, the communication quality is good without connecting MPA. The points on the constellation diagram are accurately located near the symbol mapping points. Due to the MPA NLT, the constellation points are remarkably affected, spreading, shifting, or deforming. The relative distance between the points and symbol mapping points increases, leading to larger phase errors and rapid degradation in communication quality.

5.3. Discussion on the NL Influence of on the Wireless Communication Signal EVM

After the previously described test, the Summary-EVM and Frame Summary data were combined for all selected channels and signals. The EVM root mean square (RMS) for all selected channels and signals were calculated. The downlink synchronization channels, including Primary Synchronization Signal (PSS), Secondary Synchronization Signal (SSS), and Physical Broadcast Channel (PBCH), serve the purpose of time and frequency synchronization, cell search, and carrying system broadcast information. PBCH_DMRS utilizes Demodulation Reference Signals (DMRSs) as demodulation reference pilots for the physical broadcast channel. The purpose of synchronization signals is to facilitate time and frequency synchronization as well as cell search. Meanwhile, the physical broadcast channel is designed to carry system broadcast information. The EVM of various channels in the downlink using the data without MPA is shown in Figure 11(a). It can be observed that except for the EVM at -30 dBm input signal, the various channel EVMs fluctuate within a small range. The main synchronization signal PSS and the secondary synchronization signal SSS have similar EVM values. The PBCH_DMRS with built-in demodulation reference signals shows optimization in EVM compared to the regular PBCH. We emphasize from Figure 11(b) that when the MPA operates in the linear region, the EVMs of PSS, SSS, PBCH, and PBCH_DMRS channels fluctuate smoothly lower than 1% RMS. However, as the IM3 com-

FIGURE 10. VSA software testing interface.

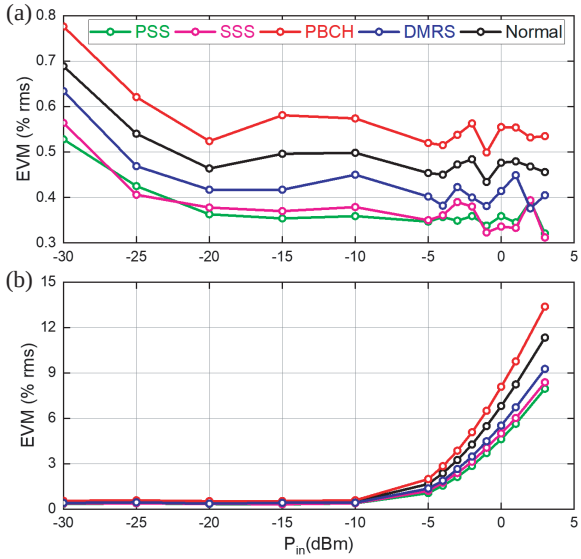

FIGURE 11. EVM of various channels in the downlink link vs input signal power (a) without and (b) with MPA.

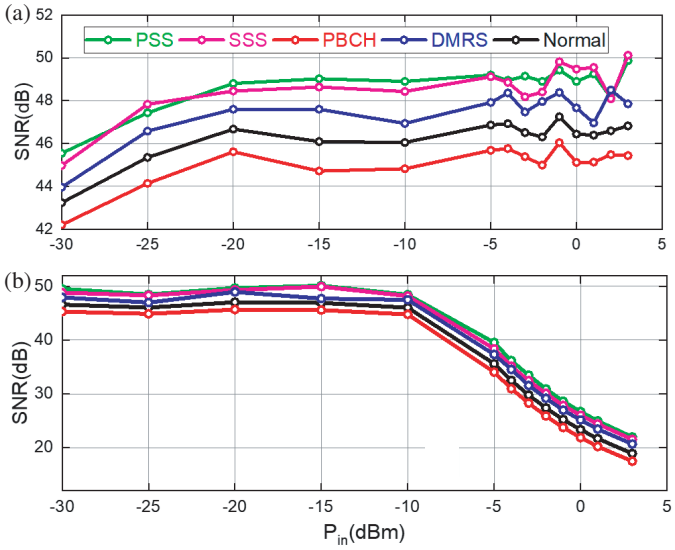

FIGURE 12. SNR of various channels in the downlink link vs input signal power (a) without and (b) with MPA.

ponents begins to appear and as the MPA gradually works its way through the NL region, the IM3 components signal power rises rapidly, and the EVM of the signal gradually increases at a fast rate.

5.4. Discussion on EMI Effect from SNR

The SNR is derived from the EVM from the conversion relationship given by:

$$SNR_{\text{dB}} = 20\log 10^{\left(\frac{100}{EVM_{rms}}\right)} \quad (5)$$

A relationship curve between SNR of transmitted QPSK and input signals can be plotted only by inverting the EVM. Without MPA, the SNR values as illustrated in Figure 12(a) stabilize within a certain range after a brief increase.

The peak SNR of the downlink channel is 49 dB which indicates a good communication quality in the absence of MPA. The SNRs of the two synchronization signals are close, and the PBCH with built-in demodulation reference signals has a gain of approximately 2 dB to 3 dB compared to the PBCH without demodulation reference signals. Eventually, the SNR drops below 25 dB due to the MPA NLT effect as illustrated by Figure 12(b), indicating a substantial presence of noise and interference in the communication channel. In other word, we can state that when the MPA operates in the linear region, the PSS, SSS, PBCH, and PBCH_DMRS channels present SNR rather constant greater than 25 dB. However, when the IM3 component begins to appear and the IM3 components power rises rapidly as the MPA progressively operates in the NL region, the SNR decreases logarithmically.

6. CONCLUSION

An experimental study of undesirable EMI dedicated to the 802.11b IEEE wireless communication system by considering the MPA undesirable NL effect is studied. The developed empirical characterization methodology guiding the elaboration of the experimental setup is described with the employed equipment specifications. The NLT characterization is based on the experimental assessment of the gain, P1dB, and IM3 parameters.

To perform the EMI analysis, downlink synchronization and physical broadcast channels as PSS, SSS, PBCH, and PBCH_DMRS are considered. The EMI effect due to the MPA NLT is assessed from the SNR of QPSK communication signal. Considering the signal modulation, the EMI of the MPA NLT reduces the system signal-to-noise ratio by 20 dB. Without MPA, the SNR peak in the downstream channel reaches 49 dB. The main synchronization signal PSS and secondary synchronization signal SSS exhibit similar EVM and SNR, with marginal differences. The internal demodulation reference signal PBCH shows optimized EVM and SNR compared to the regular PBCH.

The developed test technique is useful in the RFI analyses of 6G future communication system.

ACKNOWLEDGEMENT

The research was carried out within the framework of joint project with the support of the National Key Research and Development Program of China (2022YFE0122700) and the Belarusian Republican Foundation for Fundamental Research(T22KITG-018).

REFERENCES

[1] Saad, W., M. Bennis, and M. Chen, "A vision of 6G wireless systems: Applications, trends, technologies, and open research problems," *IEEE Network*, Vol. 34, No. 3, 134–142, 2019.

[2] Mordachev, V., E. Sinkevich, Y. Yatskevich, A. Krachko, P. Zaharov, and X. Ma, "Simulation of nonlinear interference in aircraft systems operating in complex electromagnetic environment created by land-based and air-based wireless systems," in *2017 International Symposium on Electromagnetic Compatibility — EMC Europe*, 1–6, Angers, France, 2017.

[3] Sinkevich, E. V., "Discrete nonlinear simulation of radio receivers for electromagnetic compatibility analysis and design: Estimation of the signal-to-interference ratio," in *2007 7th International Symposium on Electromagnetic Compatibility and Electromagnetic Ecology*, 166–169, St. Petersburg, Russia, 2007.

[4] Bayram, Y., J. L. Volakis, S. K. Myoung, S. J. Doo, and P. Roblin, "High-power EMI on RF amplifier and digital modulation schemes," *IEEE Transactions on Electromagnetic Compatibility*, Vol. 50, No. 4, 849–860, 2008.

[5] Wiklundh, K. and P. Stenumgaard, "EMC challenges with 6G," in *2022 International Symposium on Electromagnetic Compatibility — EMC Europe*, 19–24, Gothenburg, Sweden, 2022.

[6] Wiklundh, K. and P. Stenumgaard, "EMC challenges for the era of massive internet of things," *IEEE Electromagnetic Compatibility Magazine*, Vol. 8, No. 2, 65–74, 2019.

[7] Yaklaf, S. K. A. A., K. S. Tarmissi, and N. A. A. Shashoa, "6G mobile communications systems: Requirements, specifications, challenges, applications, and technologies," in *2021 IEEE 1st International Maghreb Meeting of The Conference on Sciences and Techniques of Automatic Control and Computer Engineering MI-STA*, 679–683, Tripoli, Libya, 2021.

[8] Pareschi, F., R. Rovatti, and G. Setti, "EMI reduction via spread spectrum in DC/DC converters: State of the art, optimization, and tradeoffs," *IEEE Access*, Vol. 3, 2857–2874, 2016.

[9] Auer, M. and T. Karaca, "Spread spectrum techniques for class-D audio amplifiers to reduce EMI," *E & I Elektrotechnik Und Informationstechnik*, Vol. 1, No. 133, 43–47, 2016.

[10] Jin, C., M. T. Tan, and K. Y. See, "Filterless class-D amplifier with pseudorandomized carrier frequency modulation for EMI reduction," *IEEE Transactions on Electromagnetic Compatibility*, Vol. 55, No. 1, 74–80, 2012.

[11] Mrad, R., G. Pillonnet, F. Morel, C. Vollaire, and A. Nagari, "Predicting the impact of magnetic components used for EMI suppression on the base-band of a power amplifier," *IEEE Transactions on Power Electronics*, Vol. 30, No. 8, 4199–4208, 2015.

[12] Liu, R., L. Qi, and A. Zhu, "A linearity-improved 24-29-GHz GaN MMIC doherty power amplifier with reconfigurable self-adaptive peaking gate bias network," *IEEE Transactions on Microwave Theory and Techniques*, 1–14, 2024.

[13] Fuchs, E., T. Handte, D. Verenzuela, and S. T. Brink, "Optimized sequences for estimation of power amplifier nonlinearity in 802.11 wireless LAN," in *2024 IEEE Wireless Communications and Networking Conference (WCNC)*, 01–06, Dubai, United Arab Emirates, 2024.

[14] Jadidi, M. M., A. M. Khoueini, A. Mohammadi, and V. Meghdadi, "Performance analysis and power allocation for uplink cell-free massive MIMO system with nonlinear power amplifier," *IEEE Transactions on Communications*, 1–1, 2024.

[15] Fiori, F., "A new nonlinear model of EMI-induced distortion phenomena in feedback CMOS operational amplifiers," *IEEE Transactions on Electromagnetic Compatibility*, Vol. 44, No. 4, 495–502, 2002.

[16] Yeh, M.-L., W.-R. Liou, H.-P. Hsieh, and Y.-J. Lin, "An electromagnetic interference (EMI) reduced high-efficiency switching power amplifier," *IEEE Transactions on Power Electronics*, Vol. 25, No. 3, 710–718, 2009.

[17] Filion, B., A. T. Nguyen, L. A. Rusch, and S. LaRochelle, "Post-compensation of nonlinear distortions of 64-QAM signals in a semiconductor-based wavelength converter," *Journal of Lightwave Technology*, Vol. 34, No. 9, 2127–2138, 2016.

[18] Palumbo, G. and S. Pennisi, "High-frequency harmonic distortion in feedback amplifiers: Analysis and applications," *IEEE Transactions on Circuits and Systems I: Fundamental Theory and Applications*, Vol. 50, No. 3, 328–340, 2003.

[19] Maffezzoni, P., "Efficient multiparameter sensitivity computation of amplifier harmonic distortion," *IEEE Transactions on Circuits and Systems Ii: Express Briefs*, Vol. 54, No. 3, 257–261, 2007.

[20] Miao, Y. and Y. Zhang, "Distortion modeling of feedback two-stage amplifier compensated with miller capacitor and nulling resistor," *IEEE Transactions on Circuits and Systems I: Regular Papers*, Vol. 59, No. 1, 93–105, 2011.

[21] Shi, G., "Symbolic distortion analysis of multistage amplifiers," *IEEE Transactions on Circuits and Systems I: Regular Papers*, Vol. 66, No. 1, 369–382, 2018.

[22] Baxevanakis, D. and P. P. Sotiriadis, "A general time-domain method for harmonic distortion estimation in CMOS circuits," *IEEE Transactions on Computer-Aided Design of Integrated Circuits and Systems*, Vol. 40, No. 1, 157–170, 2020.

[23] Celik, A., Z. Zhang, and P. P. Sotiriadis, "A state-space approach to intermodulation distortion estimation in fully balanced bandpass G_m–C filters with weak nonlinearities," *IEEE Transactions on Circuits and Systems I: Regular Papers*, Vol. 54, No. 4, 829–844, 2007.

[24] Pini, G., D. Manstretta, and R. Castello, "Analysis and design of a 20-MHz bandwidth, 50.5-dBm OOB-IIP3, and 5.4-mW TIA for SAW for saw-less receivers," *IEEE Journal of Solid-state Circuits*, Vol. 53, No. 5, 1468–1480, 2018.

[25] Zhou, Y., F. Hutu, G. Villemaud, and T. Riihonen, "Nonlinear power amplifier effects on a full duplex spatial modulation system," in *2021 IEEE 32nd Annual International Symposium on Personal, Indoor and Mobile Radio Communications (PIMRC)*, 824–828, Helsinki, Finland, 2021.

[26] Sharma, S., A. Singh, K. Deka, and C. Adjih, "Impact of nonlinear power amplifier on ber performance of OTFS modulation," in *2023 IEEE International Conference on Advanced Networks and Telecommunications Systems (ANTS)*, 627–632, Jaipur, India, 2023.

[27] Jing, X. and Z. Xiao, "A novel characteristic parameter approach for analysis and design of linear components in nonlinear systems," *IEEE Transactions on Signal Processing*, Vol. 64, No. 10, 2528–2540, 2016.

[28] Fiori, F., "EMI-induced distortion of baseband signals in current feedback instrumentation amplifiers," *IEEE Transactions on Electromagnetic Compatibility*, Vol. 60, No. 3, 605–612, 2017.

[29] Fiori, F. L. and P. S. Crovetti, "Prediction of high-power EMI effects in CMOS operational amplifiers," *IEEE Transactions on Electromagnetic Compatibility*, Vol. 48, No. 1, 153–160, 2006.

[30] Golubovich, D. and S. Chermoshentsev, "Virtual testing of the emission of electromagnetic interference from electronic means according to the electromagnetic compatibility requirements," in *2019 International Conference on Electrotechnical Complexes and Systems (ICOECS)*, 1–4, Ufa, Russia, 2019.

[31] Parvis, M., G. Perrone, and A. Vallan, "A precompliance EMC test-set based on a sampling oscilloscope," *IEEE Transactions on Instrumentation and Measurement*, Vol. 52, No. 4, 1220–1223, 2003.

[32] Mordachev, V. and E. Sinkevich, "Experimental analysis of radio receiver susceptibility to out-of-band interference by means of double-frequency test system," in *10th International Symposium on Electromagnetic Compatibility*, 405–411, York, UK, 2011.

[33] Sinkevich, E. and V. Mordachev, "Investigation of the transmitter susceptibility to reverse intermodulation by the use of double-frequency diagrams," in *2015 IEEE International Symposium on Electromagnetic Compatibility (EMC)*, 1159–1164, Dresden, Germany, 2015.